IMAGING SINGLE CELLS IN A BEAM OF LIVE CYANOBACTERIA WITH AN X-RAY LASER

Gijs van der Schot[1#], Martin Svenda[1#], Filipe R. N. C. Maia[1,2], Max Hantke[1], Daniel P. DePonte[3,4], M. Marvin Seibert[1,4], Andrew Aquila[3,5], Joachim Schulz[3,5], Richard Kirian[3], Mengning Liang[3], Francesco Stellato[3,6], Bianca Iwan[1], Jakob Andreasson[1], Nicusor Timneanu[1], Daniel Westphal[1], F. Nunes Almeida[1], Dusko Odic[1], Dirk Hasse[1], Gunilla H. Carlsson[1], Daniel S. D. Larsson[1], Anton Barty[2], Andrew V. Martin[3,7], Sebastian Schorb[4], Christoph Bostedt[4], John D. Bozek[4], Daniel Rolles[3], Artem Rudenko[3,8], Sascha Epp[3], Robert Hartmann[9], Nils Kimmel[9,10], Ne-Te Duane Loh[11], Henry N. Chapman[3,12], Inger Andersson[1], Janos Hajdu[1,5*], Tomas Ekeberg[1*]

[1] Laboratory of Molecular Biophysics, Department of Cell and Molecular Biology, Uppsala University, Husargatan 3 (Box 596), SE-751 24 Uppsala, Sweden.
[2] NERSC, Lawrence Berkeley National Laboratory, Berkeley, California, USA.
[3] Center for Free-Electron Laser Science, DESY, Notkestrasse 85, 22607 Hamburg, Germany.
[4] LCLS, SLAC National Accelerator Laboratory, 2575 Sand Hill Road, Menlo Park, California 94025, USA.
[5] The European XFEL GmbH, Albert-Einstein-Ring 19, 22761 Hamburg, Germany.
[6] I.N.F.N. and Physics Department, University of Rome 'Tor Vergata', Via della Ricerca Scientifica 1, 00133, Rome, Italy.
[7] ARC Centre of Excellence for Coherent X-ray Science, School of Physics, University of Melbourne, Parkville, Victoria 3010, Australia.
[8] Department of Physics, Kansas State University, 331 Cardwell Hall, Manhattan, Kansas 66506, USA.
[9] PNSensor GmbH, Römerstrasse 28, 80803 München, Germany.
[10] Max Planck Institute for Extraterrestrial Physics, Giessenbachstrasse, 85741 Garching, Germany.
[11] Centre for BioImaging Sciences, National University of Singapore, 14 Science Drive 4, Singapore 117557, Singapore.
[12] University of Hamburg, Notkestrasse 85, 22607 Hamburg, Germany.

#These authors constributed equally to the project.
* Corresponding authors: Janos Hajdu: janos@xray.bmc.uu.se, Tomas Ekeberg: ekeberg@xray.bmc.uu.se

There exists a conspicuous gap of knowledge about the organisation of life at mesoscopic levels. Ultra-fast coherent diffractive imaging with X-ray free-electron lasers can probe structures at the relevant length scales and may reach sub-nanometer resolution on micron-sized living cells. Here we show that we can introduce a beam of aerosolised cyanobacteria into the focus of the Linac Coherent Light Source (LCLS) and record diffraction patterns from individual living cells at very low noise levels and at high hit ratios. We derive two-dimensional projection images directly from the diffraction patterns, and present the results as synthetic X-ray Nomarski images calculated from the complex-valued reconstructions. In another experiment, we demonstrate that it is possible to record diffraction data to nanometer resolution on live cells with X-ray lasers. Extension to sub-nanometer resolution is within reach although improvements in pulse parameters and X-ray area detectors will be necessary to unlock this potential.

Introduction
Imaging live cells at a resolution higher than the resolution of optical microscopy is a challenge. Fluorescence microscopy can achieve a degree of super-resolution via labeling with a dye, but only on the labeled regions of the cell. Electron microscopy and zone-plate X-ray microscopy[1] freeze cells to keep them motionless during image acquisition, and these cells are not alive when imaged.

X-ray lasers permit structural studies on large objects, like living cells, without modification to the sample such as freezing, sectioning, labeling, or staining. Flash diffractive imaging "freezes" motion at room temperature by using ultrashort and extremely bright coherent X-

ray pulses from an X-ray laser. Such pulses offer the possibility to outrun key damage processes[2-4] to capture a diffraction pattern from a cell which is alive at the time the intense and ultra-short X-ray pulse traverses the cell. Recent results show the feasibility of this "diffraction-before-destruction" principle[2] on a variety of biological samples[5-7]. Simulations by Bergh et al.[3] suggest that diffraction data to sub-nanometer resolution may be collected on micron-sized living cells, and in the present study, we explore the feasibility of this promise experimentally.

We first demonstrate that live cyanobacteria can be efficiently aerosolised, and a beam of live cells can be introduced into the pulse train of an X-ray laser at a reduced pressure. We show that we can record high-quality diffraction patterns on such cells with practically no scattered background. We retrieve phases directly from the diffraction patterns to reconstruct images, using a variant[8] of the Gerchberg-Saxton-Fienup phase retrieval algorithm[9-10] and present the reconstructed exit-wave fronts as synthetic X-ray Nomarski images[11] in a similar manner to what one would expect to see in a Nomarski microscope, only at the higher resolutions available using X-rays. Finally, we present experimental evidence that diffraction data to nanometer resolution can be recorded on live cells.

Results

Live cells
Cyanobium gracile and *Synechococcus elongatus* cells were selected for these studies because of their small size, robustness, and convenient autofluorescence properties that can be used to assess cell viability[12]. Cyanobacteria are tough and can be found in hot and cold environments, including volcanic regions and the polar ice caps. Solitary *C. gracile* and *S. elongatus* cells have an oval-to-cylindrical shape, and vary in size between 0.25-0.4 μm in diameter and 0.4-4.0 μm in length[13]. Cell division occurs symmetrically by binary fission. The two daughter cells separate from each other after reaching the size and shape of the mother cell[14]. We used non-synchronised cell cultures undergoing active growth to provide cells in various stages of their cell cycle. Injected cells arrive in random order and are imaged in random orientations.

Aerosol sample injection
Aerosol injection[7,15] delivers samples without any container and is capable of producing millions of shots per day for high-throughput studies at low noise levels. Other methods employ membranes[9] or closed containers[15]. Everything that is illuminated by a pulse of an X-ray laser is "sample" in coherent diffractive imaging, including the structure of the sample holder, the liquid column of a liquid jet, or materials that make up microfluidic devices. Such sample holders contribute to scattering and increase unwanted noise. Aerosol injection removes this clutter and assures that the sample is clearly isolated from its surroundings, which is important for phasing.

Aerosols play various roles in biology. A large number of infectious diseases are transmitted via aerosols. Ocean sprays put out about 3.5×10^{12} kg aerosol per year from jet drops formed when bubbles burst on wave crests[16] and can carry live cells (like those studied here) over wide areas. Aerosols are also widely used in scientific and medical applications. A recent study shows that bio-electrosprayed multicellular zebrafish embryos are viable and develop normally[17]. Cell sorters use microdroplets to separate different cells from each other. Similarly, the new science of tissue printing[18-19] is based on the use of microdroplets to deliver cells to pre-defined positions. We exploit similar processes in this study to bring living cells into the gas phase for a brief period of time and to deliver these cells into the pulse train of the LCLS as a narrow beam (Figure 1).

Cells were transferred into a volatile buffer prior to aerosolisation to avoid formation of surface deposits during the evaporation of microdroplets. A variety of volatile buffers can be used to maintain pH and to provide suitable osmotic conditions. Here we used 25 mM ammonium acetate at pH 7.5. By adjusting temperature, humidity and gas flow, the amount of water on the sample can be controlled.

The suspension of live cells was aerosolised with a gas-dynamic virtual nozzle[20] with helium. In the nozzle, a converging stream of pressurised helium squeezes a 20 μm wide liquid column into a 1 μm jet. The reduction of diameter leads to fluid acceleration, and the liquid column accelerates from 0.06 m/s (in the 20 μm column) to about 100m/s (in the 1 μm jet) in a distance of about 100 μm. Inside the short acceleration zone, the fluid is moving 1 m/s faster in front of a 1 μm object than in the back of it. This occurs for a brief period (~2 microseconds) after which the jet continues as a plug flow. In contrast to fixed-diameter nozzles, the gas-dynamic nozzle is "flexible" and lets larger clumps pass. Cells are highly elastic (elastic modulus 0.2-100 kPa[21]) and are in fact orders of magnitude more elastic than a latex condom whose elastic modulus is ~2 MPa[22]. As a result, cells respond elastically to a broad range of shear conditions[23]. Some distance away from the constriction zone, the 1 μm jet breaks into droplets in a spontaneous process governed by surface tension.

Controlled evaporation of the aerosol droplets cools the sample, and the adiabatically cooled aerosol is then guided through an aerodynamic lens to produce a narrow beam of living cells as shown in Figure 1b.

Femtosecond serial nanocrystallography[6] uses these nozzles to introduce sensitive protein crystals into the X-ray beam. The difference is that we shoot our samples after the jet breaks into droplets while nanocrystallographers shoot their samples inside the jet itself.

Figures 1c and 1d show that this type of sample injection is not disruptive and the shape and the autofluorescence of the injected cells remains unchanged. This is not quite unexpected. Aerosols of cyanobacteria can be carried for long distances, and metabolically active cells have been detected at altitudes of 20-70 km where atmospheric pressure drops to below a millibar[24-26]. We also tested the survival of E. coli cells by capturing and culturing injected cells (FNA, unpublished). The results show that E. coli cells survive the process of sample injection. One of us (R.K.) injected brewers yeast, collected it, and subsequently demonstrated anaerobic metabolism and growth (R.K. unpublished). Nevertheless, not all sample types may be amenable to aerosol sample injection, and cell lines should be tested prior to experiments. There is room for other methods, e.g. using the jet itself as in nanocrystallography for experiments where buffer exchange is not possible (but the excess liquid of the jet will contribute to scattering). Our long-term aim is to attempt very high-resolution studies on small living cells and this requires small and truly isolated cells without excess scattering material.
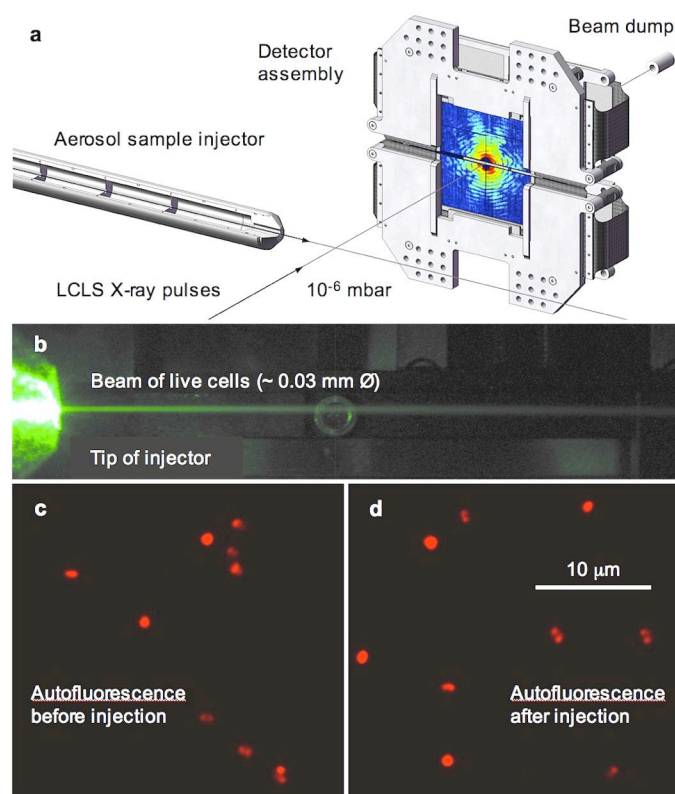
Figure 1 | The experimental arrangement. a, *C. gracile* cells were injected into the pulse train of the LCLS[27], using an aerosol sample injector built in Uppsala. The direct beam passes through an opening in the centre of the two detector halves[28]. **b**, Photograph of the beam of live cyanobacteria exiting the injector and illuminated by a green laser pointer. **c** and **d**, Fluorescence micrographs of *C. gracile* cells before **(c)** and after **(d)** injection indicate the cells remained intact. Injected cells were captured on a microscope slide in front of the injector, and the slide was transferred to atmospheric pressure to record the micrograph in **d**.

Data collection

Experiments were carried out at the Atomic, Molecular and Optics (AMO) end-station[29] of the LCLS2[7] at 517 eV (2.40 nm wavelength), or at 1,100 eV (1.13 nm) photon energy. The length of the photon bunch (full-duration at half-maximum) was about 70 fs (see Methods). The pulse was focused to a spot of 3 μm x 7 μm (full width at half maximum). The average photon density in the focus was about 1.1×10^{11} photons/pulse/μm^2 at 517 eV, and 8.6×10^{10} photons/pulse/μm^2 at 1,100 eV. Far-field diffraction patterns were recorded on a pair of pnCCD detectors[28] in the CFEL-ASG Multi Purpose (CAMP) instrument[28]. The detectors were read out at the 120 Hz repetition rate of the LCLS.

We collected diffraction patterns of *C. gracile* cells for 60 minutes at a hit ratio of 43% and selected the 7,500 strongest hits for further analysis, using the *Cheetah* software package[30]. The diffraction pattern of a non-crystalline object is continuous (Figure 2), and phases can be recovered directly from such patterns[31-33], using an iterative process[8-10]. We used the *Hawk* software package[34] for phasing (Methods). Successful phase retrieval requires accurately measured low-resolution data. This is not a trivial problem because strong hits saturate the detectors at low diffraction angles. As a compromise, we selected medium-strong hits, which contained either no, or only a few saturated pixels while still providing data to reasonably high resolution (Figure 2, Supplementary Figure 1). These patterns were analysed for weakly-constrained modes, using methods described in ref[7]. The analysis revealed no unconstrained modes in the reconstructions.
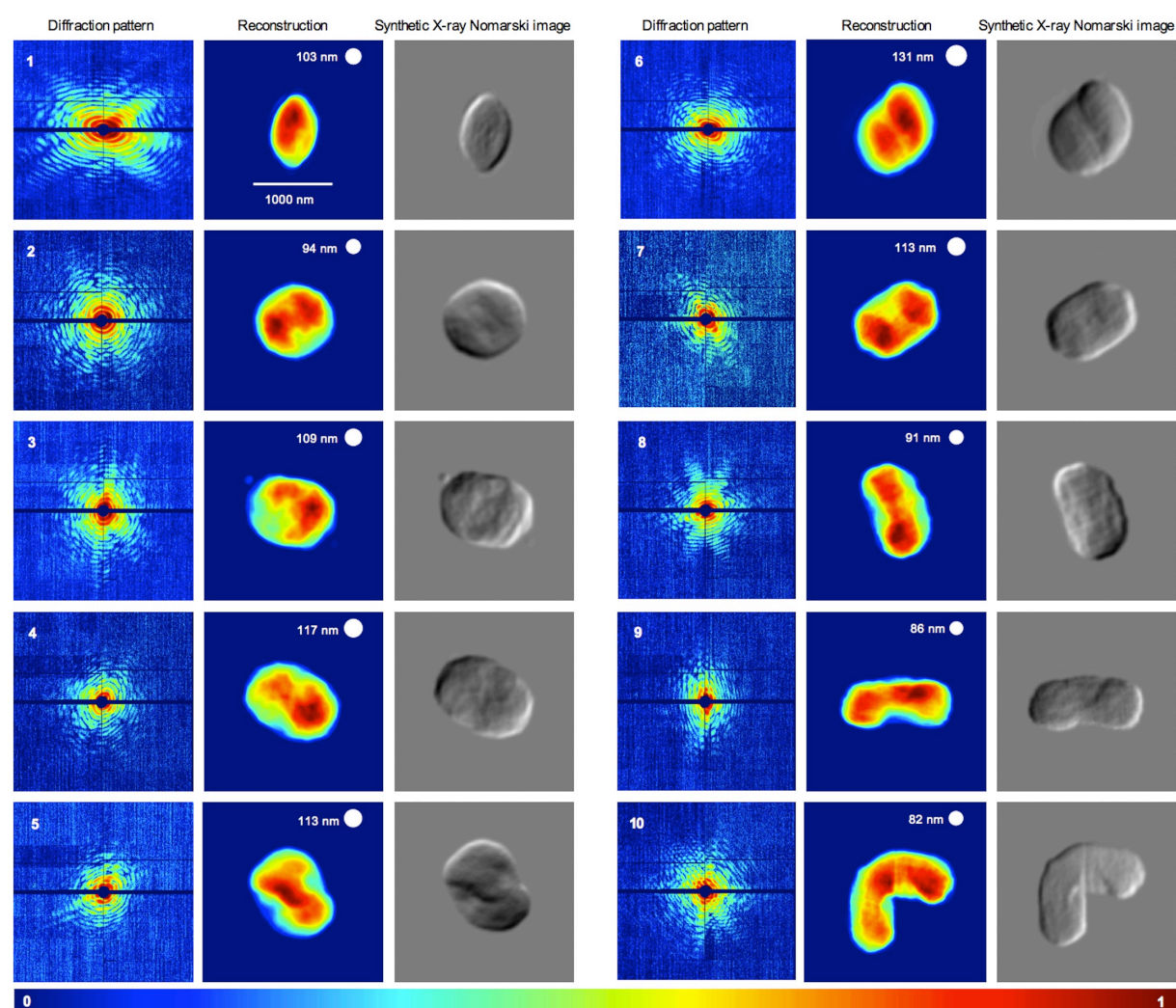
Image reconstruction

Figure 2 shows the reconstructed exit wave-fronts (images) for ten live *C. gracile* cells together with the corresponding diffraction patterns. The reconstructions represent two-dimensional projections of the electron density of the cells. The images are arranged by

increasing size, and show the expected morphologies of cells during division[13-14]. For the sake of comparison, Figure 3 shows live *C. gracile* cells imaged by conventional Nomarski differential interference contrast (DIC) microscopy in an optical microscope.

Each reconstruction in Figure 2 was repeated 400 times, starting from different and independent random phases. We used hierarchical clustering and an analysis of Fourier-errors and real-space errors to assess the quality of reconstructions (Supplementary Materials). We also calculated synthetic X-ray Nomarski DIC images[11] from the complex-valued reconstructions to present the reconstructed cells in a familiar form. These X-ray Nomarski images have the same spatial resolution as the reconstructions in Figure 2, but display the object in a similar manner to what one would expect to see in a Nomarski microscope at room temperature, only at a higher resolution available using X-rays.
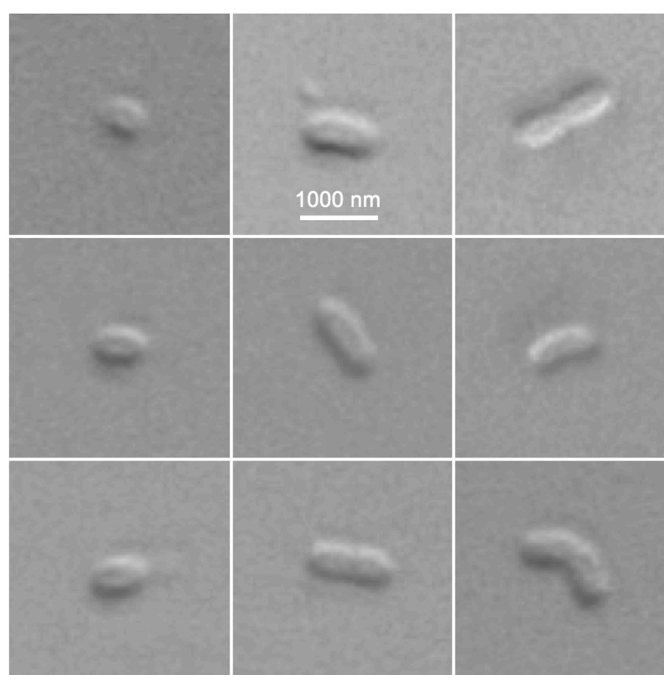
We use the phase retrieval transfer function (PRTF)[35] to assess the resolution of the reconstructions, and define resolution according to where the PRTF drops below $1/e$ (Supplementary Figure 1, refs.[4,7]). The diffraction patterns contain data to higher resolution than the resolution of the reconstructions indicated on Figure 2 (the full-period resolution at the edge of the detector was 46 nm and 33 nm in the corner at 517 eV). The results presented here show we can successfully introduce living cells into the beam of the LCLS without a container, hit them at high hit rate, and reconstruct the exit wave front from the low-noise data.

Figure 2 | Diffraction patterns, reconstructed electron densities, and synthetic X-ray Nomarski images for *C. gracile* cells. The cells were alive at the time the femtosecond pulse traversed them but exploded some picoseconds later[3,36]. Photon energy: 517 eV (water
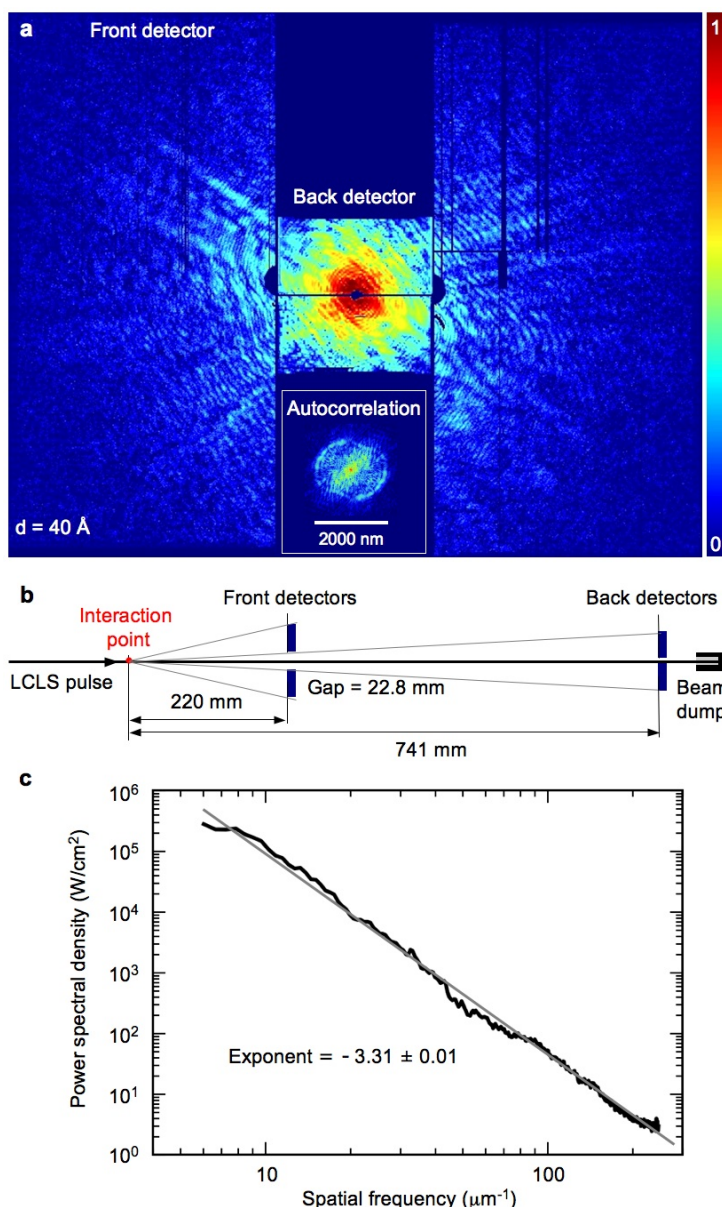
window), sample-to-detector distance: 740 mm. The total number of scattered photons in the diffractions patterns is between 0.5-5 million. Each reconstructed image is the average of up to 400 independent reconstructions (Methods and Supplementary Material). Resolution was estimated from the phase retrieval transfer function as described in Supplementary Materials. White circles in the reconstructions indicate the resolution relative to the object size. Features smaller than the circles need to be interpreted with care. Reconstructions are normalised to a 0-1 scale (colour bar), and are sorted according to cell size. Synthetic X-ray Nomarski images were calculated from the complex-valued reconstructions[11] to show the reconstructed phase shift properties of the object together with its density.

Figure 3 | Live *C. gracile* cells imaged in an optical microscope equipped with differential contrast Nomarski optics.

Reconstructions shown in Figure 2 come from relatively weak exposures that did not saturate the detectors (Methods). A number of much stronger exposures were also recorded, and in some of these exposures the diffraction signal extended to nanometer resolution. Figure 4 shows one such pattern for a live *S. elongatus* cell at 1,100 eV photon energy, 70 fs pulse length, about 10^{11} photons/μm^2 on the sample. Four pnCCD detectors were used to record this pattern (Figure 4b). The central back detector in Figure 4 is identical to the detector used in Figure 2. In this strong hit, a large part of the back detector was saturated (dark red in Figure 4a), preventing reliable phasing, but the signal extended to 4 nm resolution on the front detectors, which is the size of a small protein molecule. More than 58 million scattered photons were recorded on the back detectors, and 1.3 million on the front detectors. The size of the cell was derived from the autocorrelation. Figure 4c shows that in a log/log representation the drop-off of the signal is linear with spatial frequency, and the exponent of the signal decay is -3.31±0.01, matching simulations[37].

Figure 4 | Data extend to 4 nm full-period resolution in a strong exposure. a, Diffraction pattern of a micron-sized *S. elongatus* cell at 1,100 eV photon energy (1.13 nm wavelength) with ~10^{11} photons/μm^2 on the sample in ~70 fs. 4 nm is the size of a small protein molecule. The signal to noise ratio at 4 nm resolution was 3.7 with 0.24 photons per Nyquist pixel. The cell was alive at the time of the exposure. The central region of the pattern (dark red) is saturated and this prevented reliable image reconstruction. The pnCCDs saturate at 1,330 photons/pixel at 1,100 eV photon energy. **b**, Arrangement of four pnCCD detectors for high-resolution imaging. Each pnCCD had 1024 x 512 pixels and an active area of 76.8 mm x 38.4 mm. **c**, Signal decline with spatial frequency. The vertical scale is based on azimuthally averaged photon numbers per pixel area and corresponds to the power density in the pattern over the 70 fs exposure. The exponent of the signal decay (-3.31±0.01) matches simulations[37].

Discussion:

In synchrotron X-ray microscopy, the maximal attainable resolution on non-living biological particles is limited to about ~10 nm[38]. Unfortunately, synchrotron radiation kills live cells long before any measurable signal can be accumulated, and as a consequence, no *living* cell has ever been imaged at any reasonable resolution at a synchrotron (cells were dried, frozen, etc). "Diffraction before destruction" overcomes this problem and can give high-resolution

data, but it only permits one shot from the sample, corresponding to a spherical section through the Fourier amplitudes of the object. Three-dimensional structure determination is possible for identical objects exposed to the beam one-by-one in different orientations. This is, however, cannot be done easily with non-identical objects, such as cells.

While 3D imaging would be highly desirable, studies on living cells are based almost entirely on 2D images. Clinical and research laboratories around the world utilize two-dimensional projections of cells. The cells are usually not labeled, and their features are brought out by phase-contrast techniques in a similar manner as in our present study. Specific labeling techniques are available for X-ray diffraction microscopy, and can be used for the selective identification of components[39].

According to predictions[3], data to nanometer, sub-nanometer resolution may be recorded on micron-sized living cells through "diffraction-before-destruction"[2]. Physical limits to resolution in the pattern are related to sample size and composition, pulse duration, pulse intensity, wavelength, and the movement of the sample during exposure[2]. No fundamental limit has been encountered so far with pulses presently available from the LCLS, and the results presented here are in agreement with predictions[2,3,37]. It is, however, not trivial to image large objects, like small living cells, at high resolution.

In evaluating resolution we make a distinction between resolution in the signal and in the reconstruction. We have recorded data beyond 4 nm resolution, and reconstructed images up to resolution of 82 nm. These are still the highest resolution recordings and reconstructions of living cells using coherent diffractive imaging. In order to reach nanometer resolution in reconstructions we need to meet the following requirements.

Resolution in the signal
The diffraction signal fades away with an exponent of -3.31 (figure 4c), and accurate measurement of nanometer signal requires very low background. Container-free sample injection delivers truly isolated samples into the X-ray beam to record diffraction patterns with low scattered background. Under these conditions, signal from the sample can be measured to highest possible resolution over a flat background. The contrast between the sample and its surrounding (wet helium gas expanding into a vacuum chamber pumped to 10^{-6} mbar) is high. The clean background and the high contrast is important for the finite support constraint in phase retrieval. We estimate that nanometer resolution in the signal of a micron-sized cell would require a pulse with duration shorter than 10 fs and around 10^{12} - 10^{13} photons/μm^2 on the sample[2] at 3-10 keV photon energy.

Resolution in the reconstruction
Resolution in a two-dimensional (2D) reconstruction from a single exposure depends on the success of phase retrieval, and is also influenced by the lift-off of the Ewald sphere from the projection plane at high angles (shorter wavelengths would alleviate this problem). The projection approximation also presumes that the Born approximation is valid. This requires harder X-rays for samples thicker than those studied here.

The maximal size of an object for successful reconstruction is currently limited to about 1-2 μm at the LCLS for a number of reasons:
The bandwidth of an LCLS pulse is ~0.2 % and this gives about 500 resolution elements in an image. If a target resolution of 2 nm is aimed for, the object size cannot be bigger than about 1 μm. Smaller bandwidth would allow studies on larger objects.
Oversampling for phase retrieval requires that for each dimension, the number of pixels on the detector need to be at least twice the number of resolution elements in the image.
The focus must be large enough to cover the sample yet contain enough photons to produce strong scattered signal from the cell. A larger focus requires more photons per pulse and these extra photons are currently not available from the LCLS. This limits the maximal useful focus size, which in turn limits the object size to about 1-2 μm.
Missing low-resolution data pose perhaps the largest problem in image reconstruction. Low-resolution terms are crucial for the determination of the support for the object. The X-ray detector has a hole at its centre to let the direct beam pass through. The size of this blind spot limits the maximal object size to 1-2 μm at the relevant wavelengths. In strong

exposures, there is a further and significant loss of low-resolution data due to detector saturation as can be seen in Figure 4a.

The current limitations are technical. A femtosecond exposure "freezes" all cellular processes at room temperature, including diffusion, and thus eliminates blurring. This is an advantage over other cell-imaging methods, and will become important if or when nanometer resolution will be achieved on a micron-sized cell. Stronger and shorter pulses, like those expected from the European XFEL[40], could bring high-resolution cellular imaging within reach.

Methods

We used the *Condor* software package [http://www.github.com/mhantke/condor] to optimise experimental conditions.

Experimental Setup: The experiment was executed using the CFEL-ASG Multi-Purpose (CAMP) instrument[28], at the AMO end station[29] of the Linac Coherent Light Source (LCLS)[27]. The photon energy was 517 eV (2.40 nm wavelength) for Figure 2 and 1,100 eV (1.13 nm) for Figure 4. The bandwidth of the LCLS is about 0.5%. The length of the electron bunch was 70 fs (full-duration at half-maximum, FDHM) but the length of the photon bunch is believed to be shorter. The photon bunch contained ~1.5×10^{13} photons (1.26 mJ) at 517 eV, and 1.2×10^{13} photons (2.14 mJ) at 1100 eV. Only about 15% of the photons made it through the optics of the beam line, giving an average of about 1.1×10^{11} photons/μm^2 in the focus at 517 eV, and 8.6×10^{10} photons/μm^2 at 1100 eV. The size of the focal spot was 3 µm x 7 µm (full width at half maximum).

The CAMP chamber was equipped with two pairs of pnCCD[28] X-ray area detectors (front and back detectors), each consisting of two movable detector panels. The front detector assembly was placed 220 mm from the interaction point, and the back detector assembly at 741 mm. The direct beam exited through an opening between the two detector halves and was absorbed in a beam dump behind the detectors. Each detector panel contained 512 x 1024 pixels with 75 µm edge lengths and a full-well capacity of 500,000 electrons/pixel, corresponding to 2833 photons at 517 eV (2.40 nm) and 1333 photons at 1100 eV (1.13). The read-out rate matched the 120 Hz repetition rate of the LCLS.

Cells: *Cyanobium gracile* PCC 6307 and *Synechococcus elongatus* PCC 7942 cells were grown in Bg11 medium in batch cultures under constant light. Before the imaging experiments, cells were centrifuged at 6500 g for 10 minutes to create a soft pellet. The pellet was re-suspended in 25mM ammonium acetate, and the buffer exchange was repeated twice to remove salt and contaminants. The suspension of cells was aerosolized with helium in a gas dynamic nebuliser[20], and the cells were injected as a narrow beam into the pulse train of the LCLS.

Sample injection: The suspension of live cells was aerosolized with helium in a gas dynamic nebuliser[20], and delivered into the pulse train of the LCLS through an aerodynamic lens, using methods developed for our studies on giant viruses[7]. This method delivers cells without a container, minimizes background scattering, and can produce millions of shots per day for high-throughput studies. Most of the nebulizing gas, and vapours of the volatile buffer were pumped away through a differential pumping stage, and the concentrated and adiabatically cooled aerosol of cells was guided through an aerodynamic lens in a wet helium atmosphere, forming a narrow beam of live cells inside the vacuum chamber. The sample consumption was 2-4 µl/min from a solution of 10^{11} cells/ml. The pressure inside the chamber was 10^{-6} mbar.

Data preprocessing: The stream of raw data was monitored with the *CASS*[41] software during data collection. Subsequent processing of the raw data included background subtraction, masking of faulty pixels, and correction for non-linear detector response, a task performed by the *Cheetah* software package[30] . Electronic noise was removed by subtracting the average value of 1000 dark exposures. Bad pixels, over saturated pixels and insensitive pixels were masked out. The original patterns were down-sampled two-by-two for the reconstructions.

Hit finding was performed with the *Cheetah* software package[30] . Data were collected for 60

minutes, at a hit ratio of 43% and we selected the 7,500 strongest hits from the exposures for further analysis. Hundred "weak" patterns were then manually selected on having the least saturation, the right object dimensions, and signals extending to reasonably high resolution.

Reconstruction: Phases were retrieved with the *Hawk* software package[34]. For each pattern, 400 reconstructions were made, starting from random initial phases. These reconstructions consisted of 5000 iterations with the *RAAR* algorithm[8], using a *Shrinkwrap* algorithm[42] for support determination, and concluded with 100 iterations by the *ER* algorithm[9]. No additional constraints such as enforcing the object to be real-valued were used since we anticipate the effects of absorption in the thick cells to give effects similar to a phase object. We appreciate the fact that advanced phase retrieval algorithms such as *RAAR*[8] and *HIO*[10] are not designed to descend into the lowest point in the minimum, instead they strike a balance between the ability to identify minima and the ability to escape from shallow and presumably non-ideal minima. Therefore we always finish the phase retrieval process with a number of iterations of *Error Reduction* (*ER*)[9], which is known to guide the solution towards the lowest point of the minimum where the iterate currently resides. In our case we used 100 iterations for the ER refinement. We found that the ER refinement decreased the Fourier-error[42] by a factor of 14 on average and also improved the resolution to about two thirds compared to solutions without ER refinement.

Selection of reconstructions: We used hierarchical clustering and an analysis of Fourier-errors and real-space errors to assess the quality of reconstructions (Supplementary Materials).

Synthetic X-ray Nomarski Interference Contrast images were calculated on the basis of ideas described in ref.[11].

Optical microscopy was performed with a Zeiss AxioImager A1 fluorescence microscope equipped with Nomarski optics and a Zeiss Colibri laser source.

References

1. Cinquin, B.P. *et al.* Putting Molecules in Their Place. *J. Cell. Biochem.* **115**, 209–216 (2014).
2. Neutze, R., Wouts, R., van der Spoel, D., Weckert, E. & Hajdu, J. Potential for biomolecular imaging with femtosecond X-ray pulses. *Nature* **406**, 752-757 (2000).
3. Bergh, M. *et al.* Feasibility of imaging living cells at subnanometer resolutions by ultrafast X-ray diffraction. *Q. Rev. Biophys.* **41**, 181-204 (2008).
4. Chapman, H. N. *et al.* Femtosecond diffractive imaging with a soft-X-ray free-electron laser. *Nat. Phys.* **2**, 839–843 (2006).
5. Seibert, M.M. *et al.* Femtosecond diffractive imaging of biological cells. *J. Phys. B: At., Mol. Opt. Phys.* **43**, 194015 (2010).
6. Chapman, H. N. *et al.* Femtosecond X-ray protein nanocrystallography. *Nature* **470**, 73-77 (2011).
7. Seibert, M.M. *et al.* Single mimivirus particles intercepted and imaged with an X-ray laser. *Nature* **470**, 78-U86 (2011).
8. Luke, D.R. Relaxed averaged alternating reflections for diffraction imaging. *Inverse Problems* **21**, 37-50 (2005).
9. Gerchberg, R.W. & Saxton, W.O. Practical Algorithm for Determination of Phase from Image and Diffraction Plane Pictures. *Optik* **35**, 237-246 (1972).
10. Fienup, J.R. Reconstruction of an Object from Modulus of Its Fourier-Transform. *Opt. Lett.* **3**, 27-29 (1978).
11. Paganin, D. *et al.* X-ray omni microscopy. *J. Microsc.* **214**, 315-327 (2004).
12. Schulze, K., López, D.A., Tillich, U.M. & Frohme, M. A simple viability analysis for unicellular cyanobacteria using a new autofluorescence assay, automated microscopy, and ImageJ. *BMC Biotechnol.* **11**, 118-125 (2011).

13. Komarek, J., Kopecky J. & Cepak V. Generic characters of the simplest cyanoprokaryotes Cyanobium, Cyanobacterium and Synechococcus. *Cryptogam.: Algol.* **20**, 209-222 (1999).

14. Cohen-Bazire, G.S. Fine-Structure of Cyanobacteria. *Methods Enzymol.***167**, 157-172 (1988).

15. Bogan, M. J. et al. Single particle X-ray diffractive imaging. Nano Lett. 8, 310–316 (2008).

16. de Leeuw, G., Andreas, E.L., Anguelova, M.D. Fairall, C.W., Lewis, E.R., O'Dowd, C., Schulz, M., Schwartz, S.E., Production flux of sea spray aerosol, *Reviews of Geophysics* **49**, RG2001 (2011).

17. Clarke, J.D. and S.N. Jayasinghe, *Bio-electrosprayed multicellular zebrafish embryos are viable and develop normally.* Biomed Mater, 2008. **3**(1): p. 011001.

18. Xu, T., Jin, J., Gregory, C., Hickman, J.J., Boland, T., Inkjet printing of viable mammalian cells, *Biomaterials* **26**, 93–99 (2005).

19. Derby, B., Printing and Prototyping of Tissues and Scaffolds, *Science* **338**, 921-926 (2012).

20. DePonte, D.P. *et al.* Gas dynamic virtual nozzle for generation of microscopic droplet streams. *J. Phys. D: Appl. Phys.* **41**, 195505 (2008).

21. MacQueen, L.A., Buschmann, M.D. and Wertheimer, M.R., Mechanical properties of mammalian cells in suspension measured by electro-deformation, J. Micromech. Microeng. 20, 065007 (2010).

22. Ball, C., Krogstad, E., Chaowanachan, T., Woodrow, K.A. (2012) Drug-Eluting Fibers for HIV-1 Inhibition and Contraception. PLoS ONE 7(11): e49792. doi: 10.1371/journal.pone.0049792

23. McQueen, A., Meilhoc, E., Bailey, J.E., Flow effects on the viability and lysis of suspended mammalian cells, *Biotechnology Letters* 9, 831-836 (1987).

24. Imshenetsky, A. A., Lysenko, S. V. & Kazakov, G. A. Upper boundary of the biosphere. *Appl. Environ. Microbiol.* **35**, 1-5 (1978).

25. Griffin, D. W. Terrestrial microorganisms at an altitude of 20,000 m in Earth's atmosphere. *Aerobiologia* **20**, 135-140 (2004).

26. Womack, A. M., Bohannan, B. J. M. & Green, J. L. Biodiversity and biogeography of the atmosphere. *Philos. Trans. R. Soc.* **B365**, 3645-3653 (2010).

27. Emma, P. *et al.* First lasing and operation of an angstrom-wavelength free-electron laser. *Nat. Photonics, 2010* **4**, 641-647 (2010).

28. Struder, L. *et al.* Large-format, high-speed, X-ray pnCCDs combined with electron and ion imaging spectrometers in a multipurpose chamber for experiments at 4th generation light sources. *Nucl. Instrum. Methods Phys. Res., Sect. A* **614**, 483-496 (2010).

29. Bostedt, C. *et al*. Ultra-fast and ultra-intense x-ray sciences: first results from the Linac Coherent Light Source free-electron laser. *J. Phys. B* **46**, 164003 (2013).

30. Barty, A., et al., A new resource for processing serial X-ray diffraction data. J. Appl. Cryst. 47, 1118-1131 (2014).

31. Bernal J.D. et al. An X-ray study of chymotrypsin and hemoglobin. *Nature* **141**, 523-524 (1938).

32. Sayre, D. Some Implications of a Theorem Due to Shannon. *Acta Crystallogr.* **5**, 843-843 (1952).

33. Miao, J., Charalambous, P., Kirz, J. and Sayre, D. Extending the methodology of X-ray crystallography to allow imaging of micrometre-sized non-crystalline specimens, *Nature* **400**, 342-344 (1999).

34. Maia, F.R.N.C., *et al.* Hawk: the image reconstruction package for coherent X-ray diffractive imaging. *J. Appl. Crystallogr.* **43**, 1535-1539 (2010).

35. Chapman, H. N. *et al.* High-resolution ab initio three-dimensional x-ray diffraction microscopy. *J. Opt. Soc. Am. A* **23**, 1179 (2006b).

36. Chapman, H. N. *et al.* Femtosecond Time-Delay X-ray Holography. *Nature* **448**, 676–679 (2007).

37. Huang, X. et al., Signal-to-noise and radiation exposure considerations in conventional and diffraction x-ray microscopy. Opt Express. 17, 13541–13553 (2009).

38. Howels M.R, et al. An assessment of the resolution limitation due to radiation-damage in x-ray diffraction microscopy. J. Electron Spectrosc Rel Phenom 170:4-12 (2009).

39. Nelson, J. *et al.* High-resolution x-ray diffraction microscopy of specifically labeled yeast cells. *Proc. Natl. Acad. Sci. U. S. A.* **107,** 7235–9 (2010)

40. Evgeny A. Schneidmiller and Mikhail V. Yurkov. Photon beam properties at the European XFEL. DESY 11-152 (2011). URL: http://www-library.desy.de/preparch/desy/2011/desy11-152.pdf
41. Foucar, L., *et al.* CASS—CFEL-ASG software suite. *Comput Phys. Commun.*, **183**, 2207 – 2213 (2012).
42. Marchesini, S. *et al.* X-ray image reconstruction from a diffraction pattern alone. *Phys. Rev. B: Condens. Matter Mater. Phys.* **68**, 140101 (2003).

Supplementary Information is linked to this paper.

Author contribution statement
JH, FRNCM and TE developed the imaging concept and conceived the experiment. GvdS, FRNCM, TE, AB, NTDL, AM, and DL developed ideas and software to process the diffraction data. MS, FNA and DO prepared and characterised the cells for the study. JH, BI, DPD, MS, JA, MMS and DW developed and operated the sample injector. JDB, CB, SS, SC, NT, ML, FS, MS and MMS operated the beam line at the LCLS. RH and NK operated the pnCCD detectors. AA, JS, MH, FRNCM, TE, DL, GvdS, AB, JA, MMS, HNC, MS, ML, FS, DR, IA, AR, SE and JH characterized the imaging apparatus and carried out the experiment. GvdS, FRNCM and TE processed the data. GvdS, TE, FRNCM, and JH analysed the results. GvdS and JH wrote the manuscript with input from others.

Data deposition statement
Data will be deposited with the Coherent X-ray Imaging Data Bank (http://www.cxidb.org).

Figure captions

Figure 1 | The experimental arrangement. a, *C. gracile* cells were injected into the pulse train of the LCLS[27] at 10^{-6} mbar pressure, using an aerosol sample injector built in Uppsala. The direct beam passes through an opening in the centre of the two detector halves[28]. **b**, Photograph of the beam of live cyanobacteria exiting the injector and illuminated by a green laser beam. **c** and **d**, Fluorescence micrographs of *C. gracile* cells before **(c)** and after **(d)** injection indicate the cells remained intact. Injected cells were captured on a microscope slide in front of the injector, and the slide was transferred to atmospheric pressure to record the micrograph in **d**.

Figure 2 | Diffraction patterns, reconstructed electron densities, and synthetic X-ray Nomarski images for C. gracile cells. The cells were alive at the time the femtosecond pulse traversed them but exploded some picoseconds later[3,36]. Photon energy: 517 eV (water window), sample-to-detector distance: 740 mm. The total number of scattered photons in the diffractions patterns is between 0.5-5 million. Each reconstructed image is the average of up to 400 independent reconstructions (Methods and Supplementary Material). Resolution was estimated from the phase retrieval transfer function as described in Supplementary Materials. White circles in the reconstructions indicate the resolution relative to the object size. Features smaller than the circles need to be interpreted with care. Reconstructions are normalised to a 0-1 scale (colour bar), and are sorted according to cell size. Synthetic X-ray Nomarski images were calculated from the complex-valued reconstructions[11] to show the reconstructed phase shift properties of the object together with its density.

Figure 3 | Live *C. gracile* cells imaged in an optical microscope equipped with differential contrast Nomarski optics.

Figure 4 | Data extend to 4 nm full-period resolution in a strong exposure. a, Diffraction pattern of a micron-sized *S. elongatus* cell at 1,100 eV photon energy (1.13 nm wavelength) with $\sim 10^{11}$ photons/μm^2 on the sample in $\sim$70 fs. 4 nm is the size of a small protein molecule. The signal to noise ratio at 4 nm resolution was 3.7 with 0.24 photons per Nyquist pixel. The cell was alive at the time of the exposure. The central region of the pattern (dark red) is saturated and this prevented reliable image reconstruction. The pnCCDs saturate at 1,330 photons/pixel at 1,100 eV photon energy. **b**, Arrangement of four pnCCD detectors for high-resolution imaging. Each pnCCD had 1024 x 512 pixels and an active area of 76.8 mm x 38.4 mm. **c**, Signal decline with spatial frequency. The vertical scale is based on azimuthally averaged photon numbers per pixel area and corresponds to the power density in the pattern over the 70 fs exposure. The exponent of the signal decay (-3.31±0.01) matches simulations[37].